ATOMISTIC SIMULATION OF PLASTIC DEFORMATION MECHANISMS IN CRYSTALLINE POLYETHYLENE

by

LIPING LI

Bachelor of Science in Applied Mechanics
Huazhong Univ. of. Sci. & Tech., China (1985)

Master of Science in Engineering Mechanics
Tsinghua Univ., China (1991)

Submitted to the Department of Mechanical Engineering
in Partial Fulfillment of
the Requirements for the Degree of

MASTER OF SCIENCE IN MECHANICAL ENGINEERING

at the

MASSACHUSETTS INSTITUTE OF TECHNOLOGY

September 1994

Signature of Author_____
Department of Mechanical Engineering
August 5, 1994

Certified by_____
Mark F. Sylvester
Professor of Mechanical Engineering
Thesis Supervisor

Accepted by_____
Ain A. Sonin, Chairman
Departmental Committee on graduate Studies

ATOMISTIC SIMULATION OF PLASTIC DEFORMATION MECHANISMS IN CRYSTALLINE POLYETHYLENE

by

LIPING LI

Submitted to the Department of Mechanical Engineering
on August 5, 1994, in partial fulfillment of the
requirements for the degree of
Master of Science in Mechanical Engineering

Abstract

The atomistic details of crystalline polyethylene under strain and stress increments were studied using Molecular Dynamics, supported by use of energy minimization methods. Crystals with up to 3408 atoms have been studied for up to 200 ps at different temperatures and stress levels. A rotational defected state was found to exist at room temperature with surprising stability and it was suggested that this kind of defects could play a role in the plastic deformation process in crystalline polyethylene. The relative population of the defects in the crystals at room temperature was calculated.

The simulation results from molecular dynamics demonstrated different responses to the applied stress increments with different models (perfect model and defected model). Dislocations were generated under stresses in the model with rotational defects at a stress level as high as the ideal shear resistance of crystallographic slip. The calculations of potential energies and chain direction displacements clearly showed the onset of the slip process.

Thesis Supervisor: Mark F. Sylvester
Title: Assistant Professor of Mechanical Engineering

Acknowledgments

I wish to express my sincere thanks to Professor Mark F. Sylvester for his guidance and support in the course of this work. His insight and patience are always surprising to me. His sense of humor made life here at MIT a better memory.

I also want to thank all professors in the Mechanics and Materials group for their generous time and effort. Special thanks to Professor Mary C. Boyce for her kindness and support.

Thanks to my officemates (past and present) who helped me with various everyday problems and made my life here a lot easier. Just to name a few: Chuang-Chia Lin, Jian Cao, Clarence Chui, Suryaprakash Ganti, Christine Allan, Fred Haubensak, Manish Kothari, Srihari Balasubramanian, Leonid Lev, Vasily Bulatov and Guanshui Xu etc..

And finally , I want to thank my parents and siblings for their love through out my whole life.

Contents

List of Figures

List of Tables

Chapter 1

Introduction

1.1 Plastic Deformation in Crystalline Polymers

With combined lightness, corrosion resistance, and a good balance of stiffness and toughness maintained over a wide temperature range, polymer and polymer based materials continue to gain in importance in structural applications. In the process of fabrication of polymeric materials into useful parts, large scale plastic deformation, such as in "drawing", is usually involved. In addition, plastic deformation plays an important role in determining the use characteristics of a material. The semi-crystalline polymers are of particular technological interest because of their remarkable deformability and toughness that permit them to undergo very large permanent strains resulting in highly anisotropic properties.

The understanding of the basic mechanisms of plastic deformation of semi-crystalline polymers has been a subject of intense interest for at least the past three decades. There is a large body of experimental results characterizing the inelastic response and structural change during large deformation processes [1]. The corresponding deformation mechanisms in the crystalline part of the polymers combine crystallographic slip, mechanical twinning and stress-induced martensitic transformations, which are quite similar to those occurring in many other inorganic types of crystalline materials. Because of the long chain nature of polymers, the slip plane should contain the molecular chain since the covalent bonds in the chain backbone are much stronger

than those of the van der Waals interactions which hold neighboring chains together. However, the full details of the deformation have not been completely resolved, due to difficulties in utilizing the traditional experimental methods.

Computational prediction of polymer properties has become very important in the last a few years [2]. The modeling techniques that deal with polymers range from empirical correlation methods for bulk polymers to atomic force field methods for molecular level properties. Atomistic simulation techniques, in conjunction with experimental and theoretical approaches, have proven themselves to be useful tools for the study of polymeric materials.

1.2 Objectives of This Work

The primary purpose of this work is to initiate studies in probing the underlying microscopic mechanisms and structures which give rise to macroscopic polymer deformation through the use of atomistic simulations. Important questions, such as the identity and properties of the elemental generators of plastic strain in crystalline part of polymers and the thermodynamics and kinetics of the deformation process at the molecular level, are the first part of our interests. Hopefully this will lead to better prediction of the mechanical behavior of polymers at macroscopic level.

The following questions were the focus of this work:

- How does the crystalline polymer system respond to applied stress and strain increments?
- What is the process of crystallographic slip at the molecular level?
- What are the motions and defects in the crystal structure which lead to plastic deformation?

Polyethylene(PE), because of its structural simplicity and existence of extensive experimental data, has been the most studied system. Therefore, it was natural to make it the system investigated in this work.

1.3 Previous Work

The plastic deformation of PE has been studied on different geometric scales. This work has been recently reviewed [3]. Because of space limitation here, only the work which is related to this present work is introduced.

A large amount of experimental work has been carried out on the structure and elastic and plastic deformation of polyethylene. The presence of dislocations in polymer crystals was demonstrated from moire fringers between lamellae, and from observation through contrast effects in dark-field electron microscopy. Various patterns of dislocations were proposed by Frank *et al.* [4] and Keith and Passaglia [5], and were more extensively discussed by Predecki and Statton [6]. A dislocation model in PE was proposed by them and is shown in Figure 1-1. In crystal plasticity, it has been well established that for single slip, the slip direction in crystals always rotates toward the tensile axis, or away from the compression axis. Kiho *et al.* [7] showed that the molecular chain of polyethylene single crystals deposited on extensible substrates rotated and became tilted when the substrates were extended. Hay and Keller [8] found changes of molecular orientation from complete randomness to gradual alignment in the draw direction as a result of drawing in the bulk.

According to studies of slip traces on the surfaces of PE single crystals deformed upon Cu single crystal substrates, Gleiter and Argon [9] suggested that chain slip in polyethylene crystal could take place on any ($hk0$) plane. Of course, it should be noted that there is a significant distance between the results of single crystal and the behavior of the bulk because bulk materials are much more complicated with the existence of various different structures and defects. Experiments revealed the existence of the (100)[001] slip system [10, 8, 11] and the (010)[001] slip system [10, 8, 12] for polyethylene crystals, which can be interpreted as chain slip by the motion of screw or edge dislocations in the (100) and (010) planes, respectively. Hay and Keller [8] found the deformation took place first in the equatorial regions of polyethylene spherulite, i.e. rotation of molecular chains around the b axis occurs more readily than around the a axis. This led them to conclude that (100)[001]

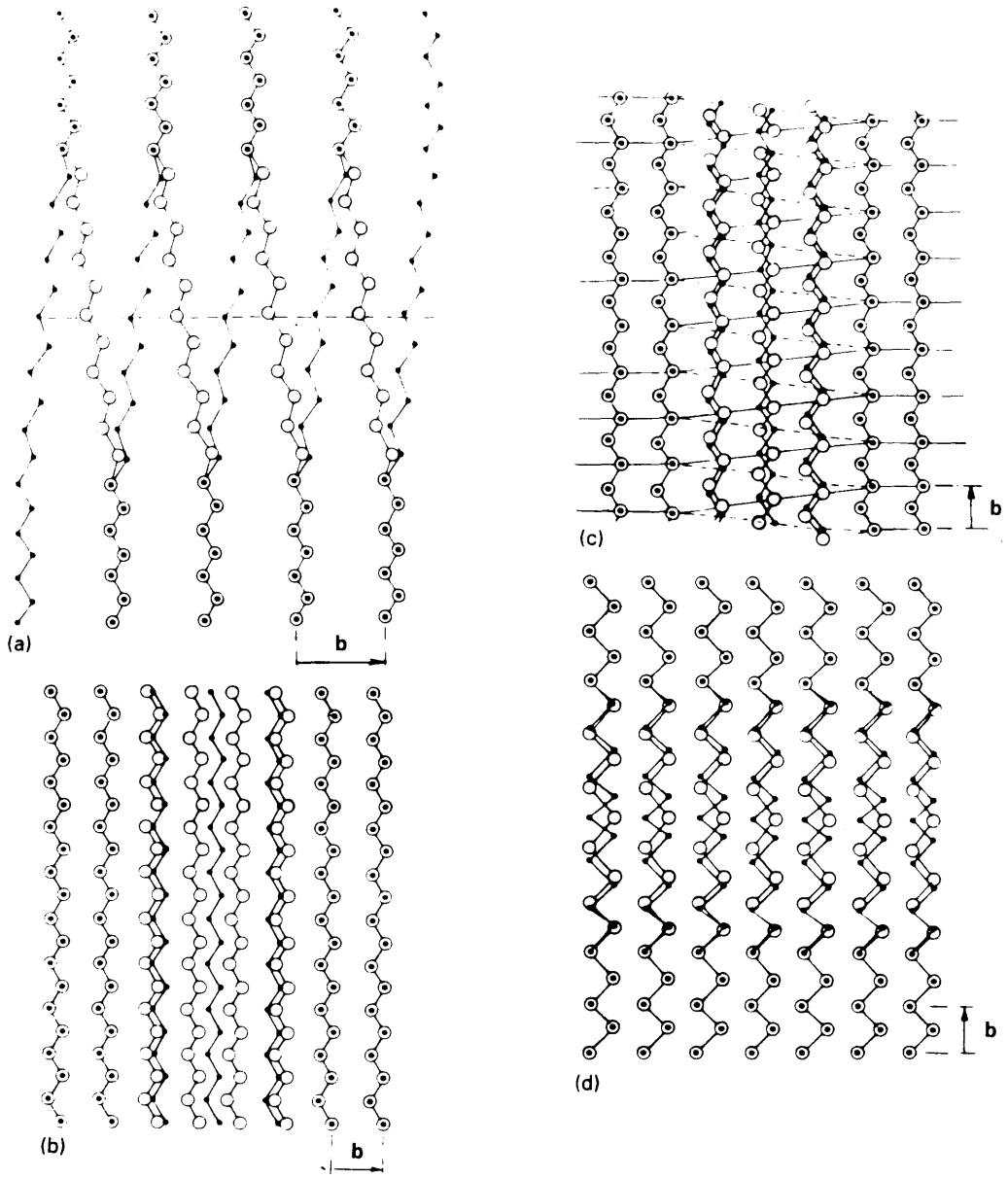

Figure 1-1: Models of dislocations on PE [3]: a) screw dislocation with a Burgers vector normal to the chain. b) edge dislocation with a Burgers vector normal to the chain. c) screw dislocation with a Burgers vector parallel the the chain. d) edge dislocation with a Burgers vector parallel to the chain.

slip was easier than (010)[001] slip. The transverse slip systems in PE crystals were studied by Frank *et al.* [4]. The closest packing direction for the transverse slip in PE crystals is the [010] direction, and then the [100] direction. Since the slip system of (010)[100] and (100)[010] are orthogonal to one another, the resolved shear stress will always be the same. This implies that the (100)[010] system will always be activated first. Slip on the (110) planes was also reported. Some investigators have attributed major importance to it [13, 51].

Previous work with computer simulation falls into two categories. First, a number of investigators have developed micromechanics based models for the macroscopic mechanical behavior of PE. Shadrake and Guiu [15] calculated the line energies of straight dislocations of various types in anisotropic PE crystals of infinite extent. It was found that screw dislocations have generally lower line energies than edges. The screw dislocation along the chain direction (slip system (100)[001]) possesses the lowest line energy which supported the results by Hay and Keller. The same model as in Shadrake and Guiu's was used by Crist [16] to analyze the yielding in terms of nucleation of [001] screw dislocations under the combined effects of temperature and stress. Peterson *et al.* [17, 18] proposed that thermal fluctuations coupled with an applied shear stress can possibly yield a workable mechanism for the initiation of screw dislocations from the edges of lamellar crystals of polymers.

Computer simulations of mechanical deformation at the molecular level have been carried out by several workers. Models based on molecular mechanics concepts have dominated work in this area. Reneker and Mazur [19] proposed a family of five crystallographic defects of three classes (two dislocations, two dispirations and one disclination). The extra energy associated with each defect in a perfect PE crystal was computed. Bacon and Geary [20] developed a model in which chain distortions are excluded and the molecular chains are straight and infinite in length. With this model, elastic constants and core structure of dislocation was investigated. Bleha *et al.* [21] calculated deformation potentials for highly extended PE chain containing simple torsional defects. Trans to gauche conformational transitions were observed during compression of all-trans chains. van der Werff and co-workers [22] investigated

the deformation energetics of static PE chain defects. It was concluded that defects inside a crystalline matrix are not weak links in PE fibers. In an investigation to the dielectric α relaxation processes in polyethylene and paraffin, Mansfield and Boyd [35] suggested that the net rotation is accomplished by means of a twisted (by 180^o) region that propagates smoothly along the chain across the crystal. It differs from previous models in that the chain torsion is relatively uniform through the twist and there is no shortening of the chain accompanying it. Argon and co-workers [23, 24] investigated the plastic deformation process in several amorphous polymer systems. In a study of atactic polypropylene, it was found that the size of a coherent plastic relaxation unit is typically 8 to 10 nm in dimensions. This was attributed to the relatively inflexible nature of backbone bonds and bond angles, permitting conformational changes only through alterations in torsional degrees of freedom.

A few molecular dynamics studies of PE and PE-like have been carried out. In a recent study by Krishna Pant *et al.* [36], they found that united atom CH_2 with Lennard-Jones nonbonded potentials commonly used for molecular dynamics simulations for polymers such as PE are inadequate. Brown and Clarke [25, 26] studied the properties of a linear polymer model resembling PE under tension over a wide temperature range. They calculated the Young's modulus for a glassy PE for $T \leq 100^oK$ and found that the modulus decreased significantly as the temperature is raised. Rychaert and Klein [27] investigated the effect of temperature on the inter-chain packing in solid n-alkanes and found that at 42^oC, in the rotator phase, there is a dramatic increase in longitudinal chain motion, each chain has four possible orientation, and a significant number of conformational defects develop, predominantly at the chain ends. Noid and co-workers [29-34] also did a series investigations on condis state, rotational isomer, conformational disorder and motion and generation of defects in crystalline PE.

Chapter 2

Simulation Methodology and Models

2.1 Simulation Techniques

2.1.1 Equations of Motion

Plastic deformation is essentially a dynamic process. Therefore, to study and understand the kinetics of the process, the Molecular Dynamics (MD) [37] method, combined with supporting energy minimizations, was used in this work.

In MD, atoms or groups of atoms are represented by point masses interacting through semi-empirical inter-atomic potentials that mimic the true quantum mechanical nature of the system. The point masses are allowed to explicitly change their positions over time by assuming that they obey the laws of classical mechanics. Lagrangians for different statistical mechanical ensembles have been developed, including microcanonical, canonical, isobaric-isothermal, isostress-isothermal ensembles. As a rule, these various Lagrangians are postulated *a priori* and then shown to generate the correct ensemble rather than developed from first principles [38]. For example, for a system with N particles, the isostress-isothermal ensemble used in this

work is:

$$\begin{aligned}\mathcal{L} &= \frac{1}{2}\sum_{i=1}^{N} m_i \xi^2 \dot{\mathbf{s}}_\mathbf{i}^\mathbf{T} \mathbf{h}^\mathbf{T} \mathbf{h} \dot{\mathbf{s}}_\mathbf{i} - \phi(\mathbf{r}) + \frac{1}{2} W Tr(\dot{\mathbf{h}}^\mathbf{T} \dot{\mathbf{h}}) - p\Omega \\ &\quad -\frac{1}{2} Tr(\mathbf{h_0^{-1}}(\sigma - p\mathbf{I})(\mathbf{h_0^T})^{-1}\Omega_0 \mathbf{h}^\mathbf{T}\mathbf{h}) + \frac{1}{2} Q\dot{\xi}^2 - f k_b T ln(\xi) \qquad (2.1)\end{aligned}$$

where the superscript T denotes the transpose of a tensor or vector, $\mathbf{s_i}$ is the unitless coordinates of the i^{th} particle within the simulation cell, m_i the i^{th} particle's mass, $\mathbf{h}$ is a 3x3 matrix whose columns are the components of the three vectors defining the simulation cell with "mass" W, ϕ, the potential energy of the particles, a function of the N particle positions ($\mathbf{r_i} = \mathbf{hs_i}$), σ the external stress applied to the system, p is the pressure ($= \frac{1}{3}Tr(\sigma)$), $\mathbf{I}$ the 3x3 identity matrix, Ω the volume of the simulation cell ($= |\mathbf{h}|$); $\mathbf{h_0}$ the initial simulation cell matrix with volume Ω_0. ξ the thermostat degree of freedom (d.o.f.) with "mass" Q describes the interaction between system and an outside fictive heat bath. T is the desired system temperature, k_b the Boltzmann's constant, and f the number of atomic d.o.f.'s in the simulation.

The terms of the Lagrangian have well-defined physical meanings. The first term is the kinetic energy of the particles. The second term is the total potential energy of the particles from sources involving the positions of two, three, and four particles. The third term represents the kinetic energy of the d.o.f.'s controlling the size and shape of the simulation cell while the fourth term expresses the PV work in changing the simulation cell's volume. The fifth term represents the potential energy of the shape of the simulation cell. The final two terms are the kinetic and potential energies of the thermostating d.o.f., respectively.

The equations of motion describing the dynamics of the atoms can be obtained from solution of Lagrange's equation and the relation between the simulation's internal "virtual" time and external "real" time, $dt' = \frac{dt}{\xi}$.

$$\ddot{\mathbf{s}}_\mathbf{i}' = -\frac{1}{m_i}\mathbf{h^{-1}}\frac{\partial \phi(\mathbf{r})}{\partial \mathbf{r_i}} - \mathbf{G^{-1}}\dot{\mathbf{G}}'\dot{\mathbf{s}}_\mathbf{i}' - \frac{\dot{\xi}'}{\xi}\dot{\mathbf{s}}_\mathbf{i}' \qquad (2.2)$$

$$\ddot{\mathbf{h}}' = \frac{\xi^2}{W}((\mathbf{\Pi} - \mathbf{pI})\mathbf{h}^{-1}\Omega - \mathbf{h}\mathbf{h}_0^{-1}(\sigma - \mathbf{pI})(\mathbf{h}_0^{\mathbf{T}})^{-1}\Omega_0) + \frac{\dot{\xi}'}{\xi}\dot{\mathbf{h}}' \tag{2.3}$$

$$\ddot{\xi}' = \frac{\xi}{Q}(\sum_{i=1}^{N} m_i \dot{\mathbf{s}}_\mathbf{i}'^{\mathbf{T}} \mathbf{G}\dot{\mathbf{s}}_\mathbf{i}' - fk_bT) - \frac{\dot{\xi}'^2}{\xi} \tag{2.4}$$

$$\mathbf{\Pi} = \frac{1}{\Omega}\sum_{i=1}^{N}(m_i\dot{\mathbf{r}}_\mathbf{i}'\dot{\mathbf{r}}_\mathbf{i}' - \frac{\partial\phi(\mathbf{r})}{\partial\mathbf{r_i}}\mathbf{r_i}) \tag{2.5}$$

where $\mathbf{r_i} = \mathbf{hs_i}$, $\mathbf{\Omega} = |\mathbf{h}|$, $\mathbf{G} = \mathbf{h}^{\mathbf{T}}\mathbf{h}$, $\mathbf{\Pi}$ =internal stress tensor.

To simulate the bulk polymer materials using a relatively small simulation cell and number of atoms, the "periodic boundary condition" (PBC), was employed to remove surface effects. In calculating the forces between atoms, the "minimum image convention" was used. This ensures proper calculation of very short range forces, such as those for covalent bonds lengths, valence angles, and torsional angles. For longer range forces, this approximation is valid only if the forces become zero, or at least very small, in a distance less than one half the span between opposing sides of the simulation cell. For the London dispersion force, which has to be considered in this work, this is a reasonable approximation.

The equations of motion form a set of $3N + 10$ coupled, nonlinear, second order differential equations which are solved as an initial value problem by using a fifth order predictor-corrector algorithm with variable time steps. Classical statistical mechanics is used to calculate macroscopic properties from trajectory of particles.

2.1.2 Potential Function for Polyethylene Model

For the PE model the inter-atomic potential function used was,

$$\phi(\mathbf{r}) = \phi^{nb} + \phi^{bl} + \phi^{\angle} + \phi^{\omega}$$

where ϕ^{nb} is the non-bonded potential term,

$$\phi_{ij}^{nb}(\mathbf{r_i}, \mathbf{r_j}) = 4\epsilon_{ij}^{o}((\frac{\sigma_{ij}^{o}}{|\mathbf{r_{ij}}|})^{12} - (\frac{\sigma_{ij}^{o}}{|\mathbf{r_{ij}}|})^{6}) \tag{2.6}$$

ϕ^{bl} is the covalent bond stretching potential,

$$\phi_{ij}^{bl}(\mathbf{r_i}, \mathbf{r_j}) = C_{ij}^{bl}(|\mathbf{r_{ij}}| - r_{ij}^0)^2 \tag{2.7}$$

$\phi^{\angle}$ the valence angle bending potential,

$$\phi_{ijk}^{\angle}(\mathbf{r_i}, \mathbf{r_j}, \mathbf{r_k}) = C_{ijk}^{\angle}(\theta_{ijk} - \theta_{ijk}^0)^2 \tag{2.8}$$

and ϕ^{ω} the backbone torsional angle rotations potential.

$$\phi_{ijkl}^{\omega}(\mathbf{r_i}, \mathbf{r_j}, \mathbf{r_k}, \mathbf{r_l}) = \frac{1}{2}C_{ijkl}^{\omega}(cos(3\omega_{ijkl}) + 1) \tag{2.9}$$

The same parameters for these potentials as in ref. [38] except C_{ijkl}^{ω}, which is the rotational energy barrier taken from ref. [39] as 2.322Kcal/mole, were used. Figure 2-1 is an explanation about the definitions of the potential functions.

2.2 Structure of Crystalline Polyethylene

X-ray diffraction gives an extremely precise description of the structure, since the crystalline polyethylene lattice diffracts X-rays as any other three dimensional lattice [41]. The single molecule in crystal of PE is a planar zig-zag structure, which is its lowest energy conformation (see Figure 2-2), with a repeat unit of $(-C_2H_4-)_n$. The straight molecules pack together like parallel rods, as indicated in Figure 2-2b which shows a plan view. The entire crystal can be generated by translations of the unit cell by lattice vectors equal to the quantities a, b, and c.

The lattice parameters for the crystal, as well as bond lengths and bond angles are as in Table 2.1 [42].

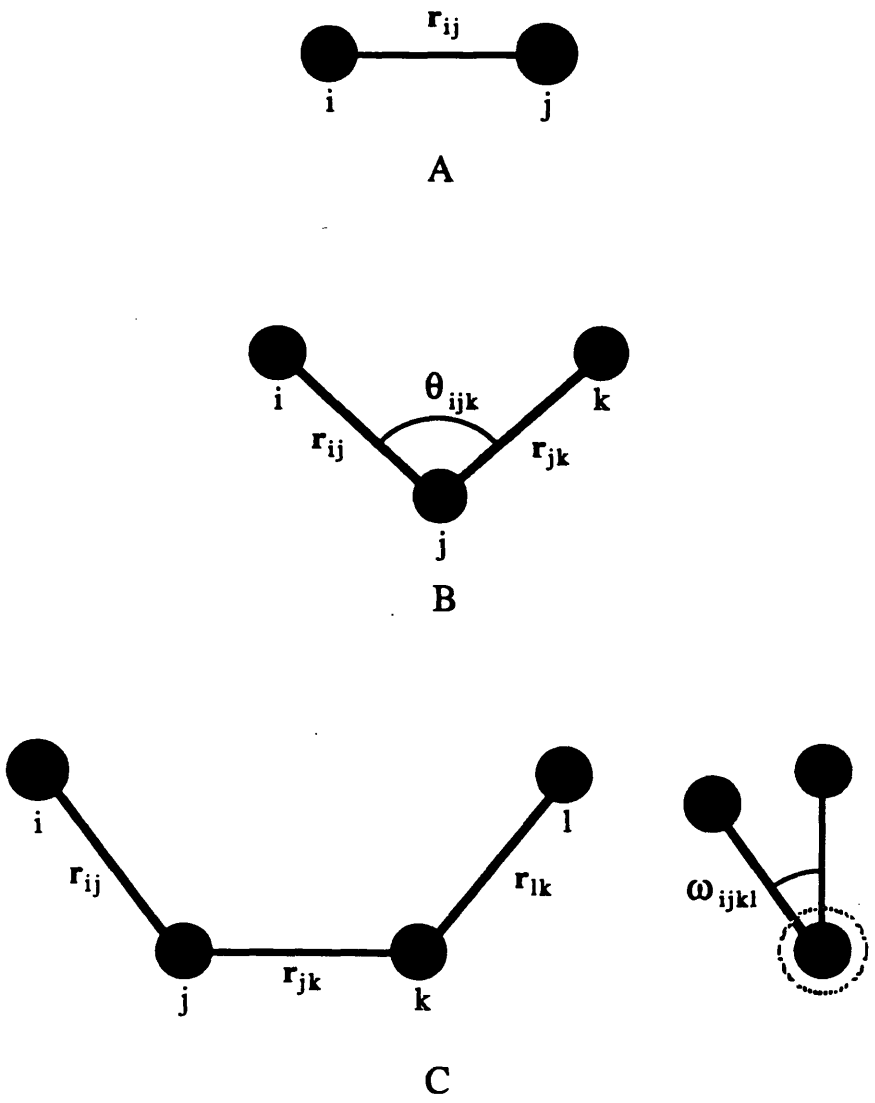

Figure 2-1: Quantities used in defining potential functions[38]: a) quantities used in defining the bond stretching potential. b) quantities used in defining the valence angle potentials. c) quantities used in defining the intrinsic backbone torsional potential.

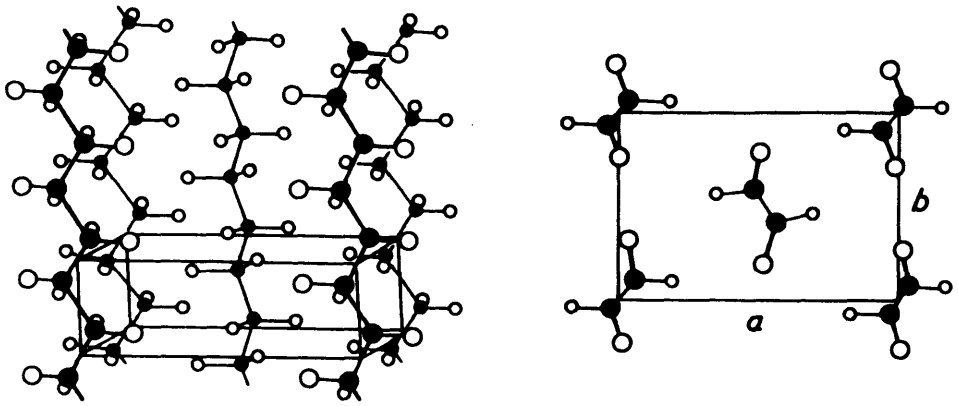

Figure 2-2: Crystal structure of orthorhombic PE [41]: a) general view of unit cell. b) Projection of unit cell parallel to the chain direction. (solid circles...carbon atoms, open circles...hydrogen atoms)

Table 2.1: Structure parameters of crystal PE

unit cell dimensions	a	b	c
($\AA$)	7.4	4.93	2.54
bond lengths	C-H	C-C	
($\AA$)	1.05	1.53	
bond angles	HCH	HCC	CCC
(degree)	109	109	112
setting angle	42^o		

2.3 Models for Simulation

2.3.1 Bilayer Chain Model

In bulk PE the lamellar thickness is on the order of a extended chain containing no more than a few hundred carbon atoms. In this work, the study of relatively short length chains was carried out for several reasons. First, the starting structure is simple and well characterized making the setting up of computer simulation code relatively straightforward. Secondly, its results can be readily compared to the experimental results, to be obtained in future work, from n-alkane single crystals of macroscopic (1 cm) dimensions.

It is believed that for the long-chain normal alkanes, the odd carbon number members of the series ranging from C_{21} to C_{27} are always orthorhombic [43]. Accordingly a bilayer chain model which contains 48 chains with each chain a $C_{23}H_{48}$ molecule giving a crystal thickness of approximately 62.31$\AA$ was built up (3408 atoms in total with each chain 71 atoms). Figure 2-3 is a projection along [001] of the CH_2 chain ends in this kind of structure. It's important to note that the simulation model in this work includes all atoms in the PE explicitly instead of using united atoms as is usually seen in the literature.

2.3.2 Infinite Chain Model

Because the difficulties encountered using the bilayer chain model (see Section 4.2), a infinite chain model was also used in this work. There are in total 24 infinite PE chains in the simulation cell, with each chain containing 22 carbon atoms (44 hydrogen atoms, 1594 atoms in total). The initial position for each single atom was taken as the ideal orthorhombic crystallographic site. Energy minimization showed that the inter-atomic potentials gives a structure in excellent agreement with the structure given by X-ray diffraction. Figure 2-4 gives a schematic representation of the infinite chain model.

One should aware the infinite chain model has two deficiencies: First of all, the

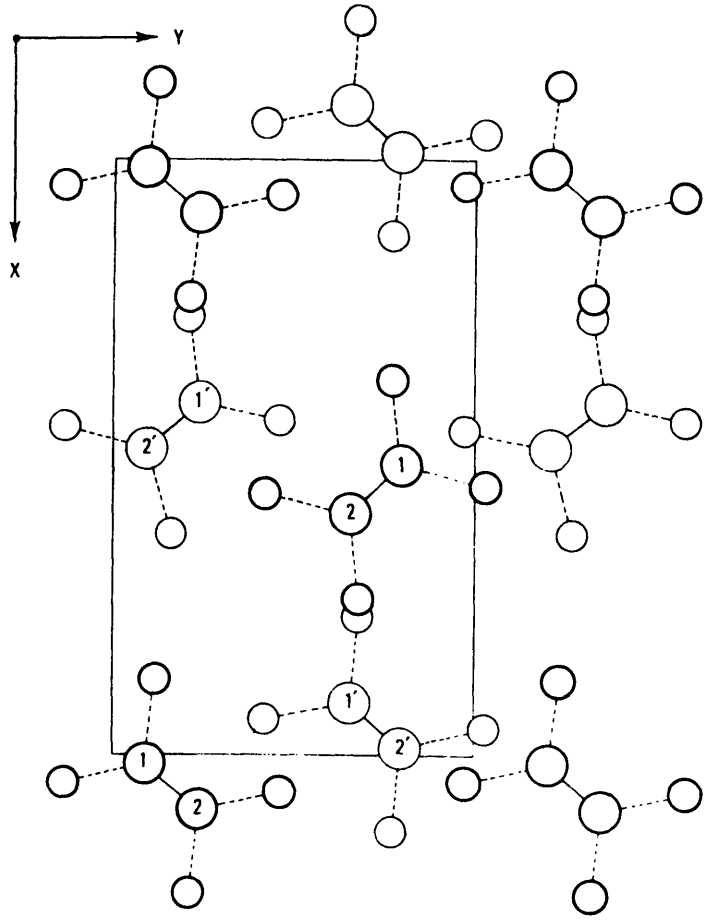

Figure 2-3: Projection along [001] of an orthorhombic structure near the (001) interface between two adjacent layers. The molecules are stacked normal to (001) and form a vertical structure [42].

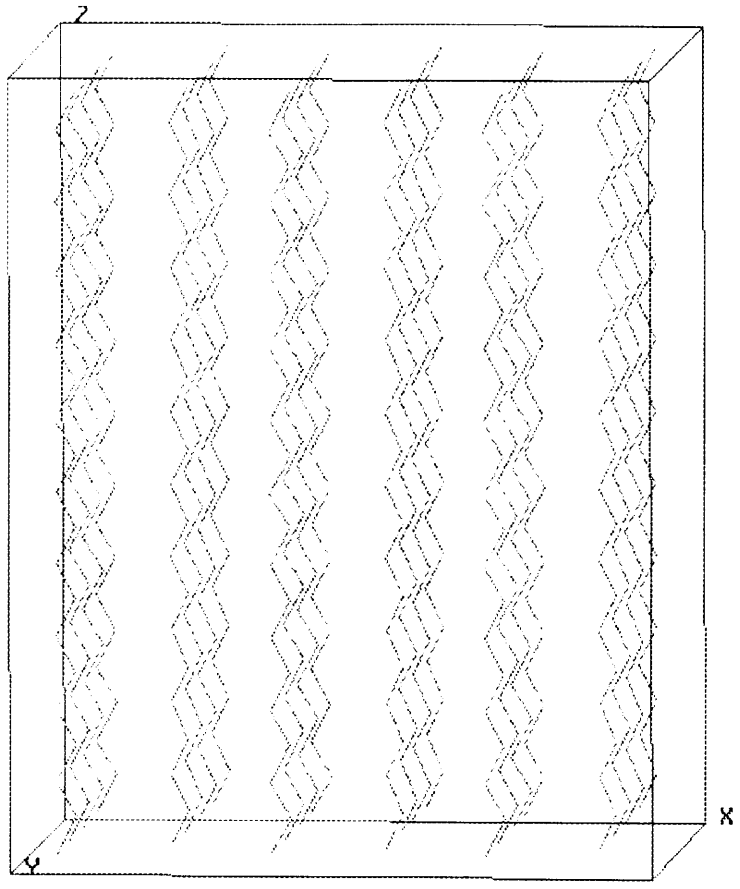

Figure 2-4: Schematic representation of the infinite chain model. Only backbones of the chains are shown in this figure (X,Y,Z directions as shown).

formation of intra-molecular defects, such as "kinks" or "jogs", will be inhibited because every chain has the same number of atoms in the infinite chain model and all chains have to extend or contract at the same fashion. And the second deficiency is that longitudinal translation will not be bounded by the presence of adjacent layers.

2.4 Equilibration from the First Starting Structure

Based on a study of Sylvester [38] on the glass transition of polypropylene (PP), the similar schedule was used to equilibrate the initially static model structure. Because of the initial structure of PE was supposed to be the perfect crystallographic structure, the equilibration process should take less time than for PP.

The mechanical equilibrium was reached as follows: At the beginning a random Maxwellian velocity distribution appropriate for the desired temperature was given. Second, run the model in a microcanonical ensemble in which occasional rescaling of the particle velocities was done to add kinetic energy into the system to bring the system close to the desired temperature. Third, run the simulation for 25 picoseconds in the canonical ensemble to continue partitioning of the kinetic energy among the modes available to the system. Fourth, run the simulation for 20 picoseconds in the isobaric-isothermal ensemble to allow the volume to relax to an equilibrium value for the system. And finally, run the simulation for a further 40 picoseconds in the isothermal-isostress ensemble to let the shape the system equilibrate to a stable value.

At the end of this process the system was in mechanical equilibrium. Properties of equilibrium can be calculated after this.

2.5 Energy Minimization

In order to investigate the possible defected states and equilibrium positions of the simulation models an energy minimization method was used in this work (see Chapter 3 for details). The conjugate gradient minimization method [40] was used. The

energies to be minimized in this case were only intra and inter molecular potential energy (no shape change of simulation cell was considered here). PBC was also used in this calculation.

Chapter 3

Chain Rotational Defects

In the process of simulation a defected state was found, in which chains rotated about their chain axis existed with a fairly high population even at room temperature. Called chain rotational defects in this work, similar states, which are sometimes called rotator phases, have been reported in n-alkanes at temperature close to the melting temperatures [27] or under α-relaxation condition[35].

3.1 Rigid Rotational Energy Barrier

Although it is almost certain that the favored method of molecular motion is far from a rigid rotation, it is still highly instructive to examine the energetics of rigid rotation in PE crystals. In this calculation, the infinite chain model was used. All the 24 chains in the simulation cell were fixed except one of them was allowed to rotate rigidly, i.e. the setting angle of this single chain was changed incrementally. Figure 3-1 is an explanation about that how the energy barrier was calculated. The top right chain (#20) is the one with rotational degree of freedom (PBC is also used here). From

$$\text{Relative Probability } \frac{f_i}{f_o} = exp(-\frac{\Delta Q^*_{io}}{kT}) \tag{3.1}$$

$$\sum_i^n f_i = 1 \tag{3.2}$$

Table 3.1: Energy barrier and minimum energy position (rigid)

position of min.(degree)	-180	-70	0	100
energy difference (Kcal/mole)	6.70	2.82	0.0	5.95
energy barrier (Kcal/mole)	14.58	6.43	29.22	35.03
equilibrium population(%)	0.001	0.787	99.208	0.004

one can calculate the expected population at a specific energy minimum relative to the stable equilibrium position. where f_i is the equilibrium probability of the system at the ith minimum, ΔQ^*_{io} the energy difference between a local minimum and the global one, k Boltzmann' s constant ($k = 1.38\text{x}10^{-23} J/K \cdot Molecule = 8.31 J/K \cdot mole$), T temperature .

The result is shown in Table 3.1 and Figure 3-2. The energy barrier reported in Table 3.1 is the energy barrier between the state shown and the next state to the right. For example, the energy barrier under column -180^o means the energy barrier between -180^o and -70^o. The calculated equilibrium population is the result at room temperature. Similar calculations are reported by Mansfield and Boyd [35] as well as McCullough [44]. In Mansfield and Boyd's calculation, an array of $C_{22}H_{46}$ molecules were used and the translational coordinate of the chains were fixed. Basically, their calculation is the same as in this work except the position of the chain rotated (they did not use PBC and the fixed chain was at the center of the system). In McCullough's calculation, a infinite chain with two rings of static PE molecules (25 chains in total) are used. The calculations in this work agree well with the results of theirs in terms of shape and have a relatively higher value because in this work the van der Waals radius of hydrogen and carbon atoms were increased by 5% or so.

3.2 Free Rotational Energy Barrier

To investigate how the other chains in the system react to the rotational defects, a different calculation from that described in Section 3.1 was carried out. In this calculation, when the single chain in section 3.1 was rotating incrementally, all other chains were allowed to rotate about their longitudinal axes and translate freely in all

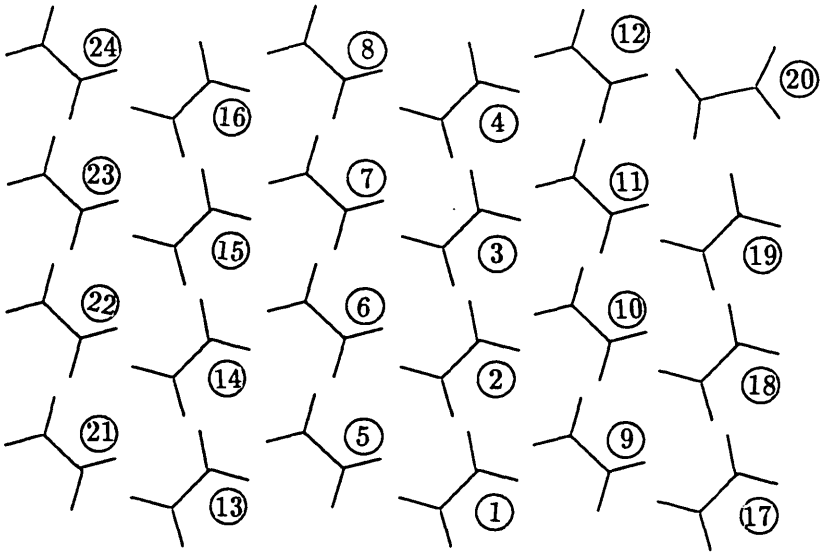

Figure 3-1: Explanation about the calculation of energy barrier. Chains are numbered for later reference. Chain #20 is the one rotated incrementally about its own axis.

Table 3.2: Energy barrier and minimum energy position (free)

position of min.(degree)	-170	-70	0	100
energy difference (Kcal/mole)	4.37	2.82	0.0	3.19
energy barrier (Kcal/mole)	5.48	4.12	6.57	6.66
equilibrium population(%)	0.054	0.783	98.754	0.409

directions to accommodate the motion of that single chain. The minimized structure showed that those chains surrounding that single rotated chain all rotated a little bit accordingly to accommodate the single chain rotation while other chains further away from that single chain did not have much movement. In this calculation, energy minimization was done to get the energy barrier. The conjugate gradient minimization method was used. The result is also shown in Figure 3-2 for comparison. From Figure 3-2, one can easily see that there are four stable rotational positions corresponding to four well-defined possible types of chain rotational defects. The energy difference between the lowest energy minimum and the adjoining minimum is 2.82Kcal/mole and the barrier between them only 4.12Kcal/mole. The equilibrium population of this chain rotational defect at room temperature can be calculated as approximately 1%. Tabulated results are shown in Table 3.2. Since the infinite chain model tends to inhibit the chain rotation because of the constraint at the chain ends, it is likely that finite length chains will rotate somewhat easier - perhaps by a mechanism such as that proposed by Mansfield and Boyd [35]. Accordingly the energy barriers between different states could be lower than those reported in this work. Actually, these kinds of defects were found in the MD simulation work and were stable for the length of the simulations. From MD simulation, it seemed that if the system has extra energy (strain or thermal), some of the chains tend to be away from their stable equilibrium position. At some stage, part of the chain would pass the energy barrier to another minimum position, and the other part of the chain would follow this tendency. This can be explained as the energy needed for the second part of the chain dragging the first part back to the original position may be higher than that needed to place the rest of the chain into the new position because of the inertia of the first part of the chain.

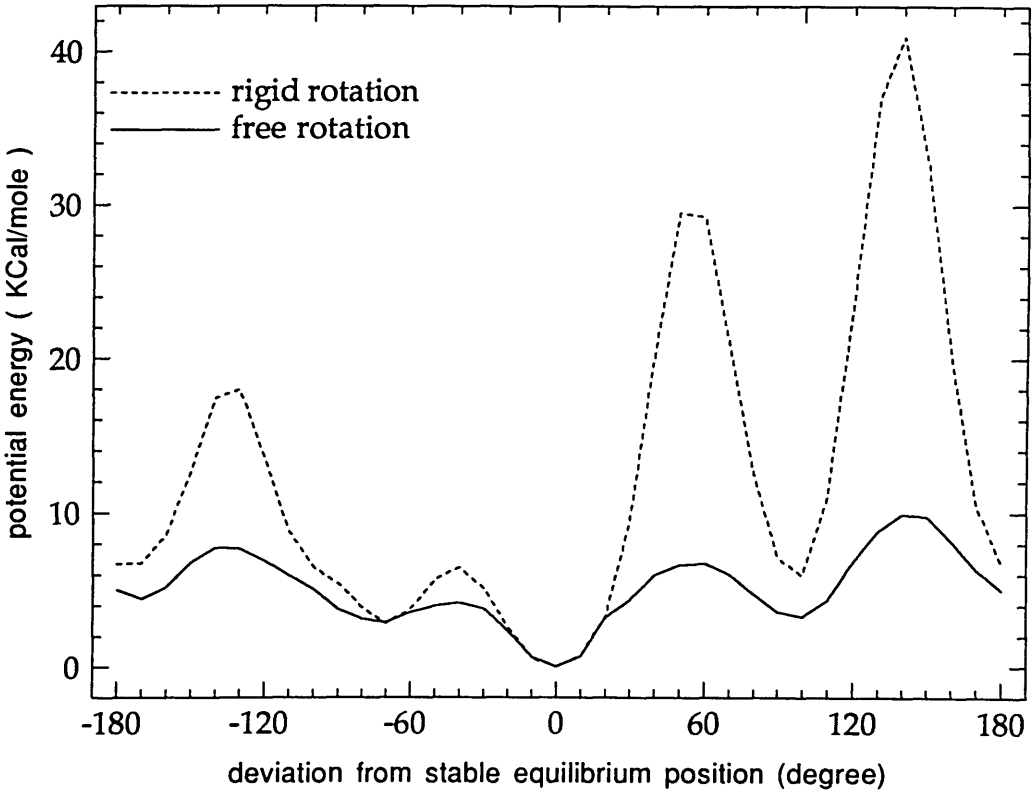

Figure 3-2: Energy barriers for single infinite chain rotation (for the energy values at each minimum position, see tables in this chapter).

The presence of significant numbers of chain rotational defects at room temperature is a new finding. This type of defect is a addition to the list of crystal defects which could play a role in plastic deformation of PE crystals.

Chapter 4

MD Simulation Results

4.1 Stress Increments Applied to the System

It was known from experiments that the easiest slip system to be activated in crystalline PE is (100)[001] which is a chain axis direction slip. In order to activate this slip system, a shear stress increment tensor was applied to the simulation cell with an average speed of $27.5MPa$ per picosecond. The stress increment applied to the system was as follows:

$$\sigma = \begin{pmatrix} 0.0 & 0.0 & \Delta\sigma \\ 0.0 & 0.0 & 0.0 \\ -\Delta\sigma & 0.0 & 0.0 \end{pmatrix}$$

After the atomic system was believed to be in mechanical equilibrium as described in Section 2.4, the stress was applied and increased until crystallographic slip was seen. 10 ps was used to let the system relax between each stress increment.

Similar strain increments have also been applied to the system, but one can get nothing but ideal inter-planar slip through this process. Actually, by changing the simulation cell shape at the beginning of each run, an imposed uniform shear strain was applied to the system. There was thus no opportunity for any chain to behave in a different way. Since ideal inter-planar shear was not the interest of this work, the

strain incrementing method was given up.

4.2 Simulation with the Bilayer Chain Model

The bilayer chain model was used at the beginning of this work because it is closer to simulating a real material – the n-alkanes. A series of simulations were done at room temperature, including shearing as described above. The shear modulus obtained from this simulation model was $12.8GPa$ which is an order of magnitude higher than the value for PE from the literature (see Table 4.1), and the yield strength was calculated as $825.16MPa$. Because there is an obvious "weak link" between layers with no constraint to the slipping of each layer relative to another, the shear observed in these experiments was found to be solely a slipping between layers rather than chain slip. It appeared the bilayer chain model can not help to get insight into the plastic deformation process by chain slip. Therefore use was made of the infinite chain model which does not have this problem.

4.3 Simulation with the Infinite Chain Model

The major simulation work was done with the infinite chain model. Different stresses were applied to the system at different temperatures. Equilibrium property calculations suggested that the infinite chain model and the inter-atomic potentials work reasonably well. The equilibrium bond lengths (except C-C bond) and bond angles are in good agreement with X-ray diffraction results. For comparison, the results of temperature dependence of lattice parameters and specific volume are shown in next section. For the rest part of this work, the results reported are from the simulations with the infinite chain model.

4.4 Temperature Dependence of Lattice Parameters and Specific Volume

The simulations were done at 233^oK, 253^oK, 273^oK and 293^oK, with the equilibration schedule described in Section 2.4. 20 ps of trajectory information was used to calculate the equilibrium properties in each simulation. The calculated temperature dependence of lattice parameters are shown in Figure 4-1. Similar results are reported by Lacks and Rutledge [45] using a molecular mechanics force field for the interatomic potential and quasi-harmonic lattice dynamics for the vibrational free energy. From Figure 4-1, one can clearly see that the results in this work are in very good agreement with their results for a and b, but for c this work obtained a relatively lower value. The experimental results of Davis *et al.* [46] are also reported in [45] for comparison. One can find that parameter a in this work is even closer to the results from the experiments and b is also in good agreement with the experimental results. c has a lower values those from the experiments. This discrepancy is from the equilibrium C-C bond length used in this work (It could be adjusted if more time were available). But the discrepancy in parameter c should not have significant effects on other equilibrium properties. As in the results from the experiments, a and b in the simulations also show an increase as the temperature increases. For parameter c, results in this work show no change, whereas the experiments show a decrease as the temperature increases. The cause of this discrepancy is the short time (20 ps) of the simulations used to obtain the property averages. The contraction in c is known to be due to low wave number lattice vibrational modes which can not be seen on a 20 ps time scale.

The result of temperature dependence of specific volume is shown in Figure 4-2. Figure 4-2 shows that the simulation results in this work are 5% lower than Maloney and Praunitz's results [47] for liquid PE, which also means the equilibrium densities for PE are higher than experimental results. It was believed that this discrepancy is probably from two reasons: One is the equilibrium C-C bond length used in the simulation as mentioned before and the other is the perfectness of the infinite chain model being used. In addition, in order to make the comparison possible, extrap-

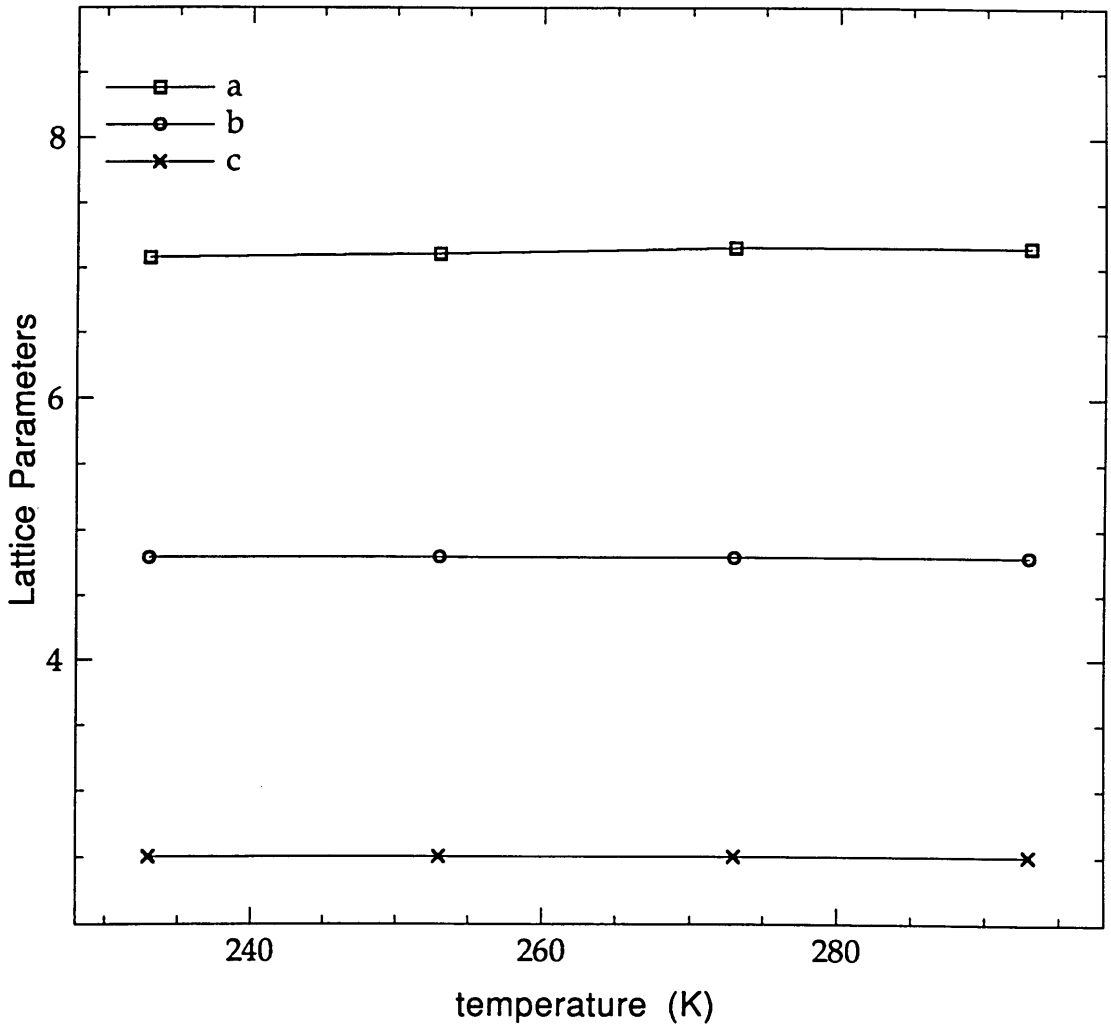

Figure 4-1: Temperature dependence of lattice parameters: a, b, c refer to lattice parameters a, b, c as usual.

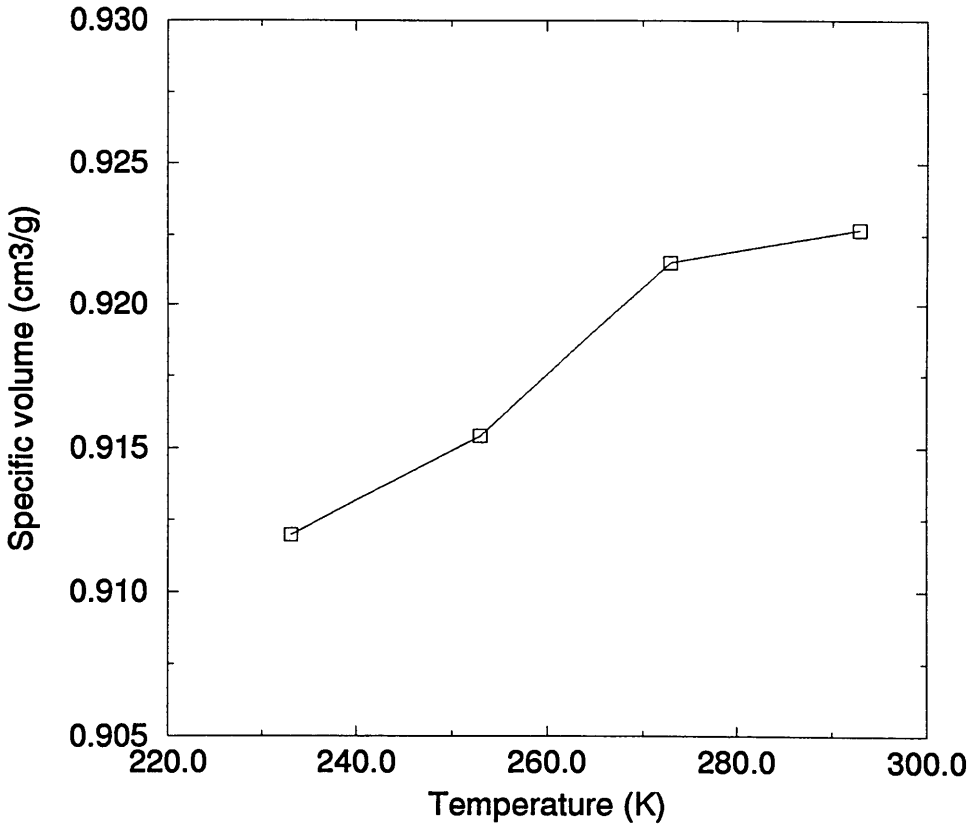

Figure 4-2: Temperature dependence of specific volume

olation of the literature results, which are obtained at a much higher temperature range ($100 - 300°C$), was done. The room temperature density from simulation is $1.04g/cm^3$ while the density calculated from the experimental unit cell dimensions is $0.988g/cm^3$. A similar calculation for amorphous PE is reported by Krishna Pant *et al.* [36] using MD, which also has a higher specific volume than from our calculation. Since this calculation is for amorphous PE, this discrepancy is not unexpected.

The volumetric thermal expansion coefficient of the material can be calculated by

$$\alpha = \frac{1}{V}\frac{dV}{dT}\Big|_p \approx \frac{1}{\overline{V}}\frac{\Delta\overline{V}}{\Delta T} \tag{4.1}$$

Since there were only four data points available, an average thermal expansion coefficient was calculated here which is $1.95\text{x}10^{-4} \pm 0.4\text{x}10^{-4}$ 1/K. Compared to the experimental results from [46] and calculated results from [45], this is a reasonable value.

4.5 Shear Modulus and Yield Stresses

The temperature dependence of shear modulus was obtained by applying stress increments described in Section 4.1 to the simulation cell and measuring the change in its shape. The result is shown in Figure 4-3. Crystalline PE is a highly anisotropic material. Nine independent constants are required to fully describe its elastic properties. The shear modulus shown here is $1/S_{55}$ which is equal to C_{55} in this case (orthorhombic structure). Some results from other researchers are shown in Table 4.1. The theoretical results shown are from lattice dynamics calculations. It was found that the shear modulus calculated in this work were well above the reported experimental range, indicating the ensemble of chains is too stiff in its response to elastic deformation. One possible explanation is the use of the perfect infinite chain model. But the "defected model" (see Section 4.6) simulation gave similar results which suggests the perfectness of the model is probably not the reason. The simulation of the bilayer chain model gave a shear modulus of $12.8GPa$ at $293°K$. This is only half of the

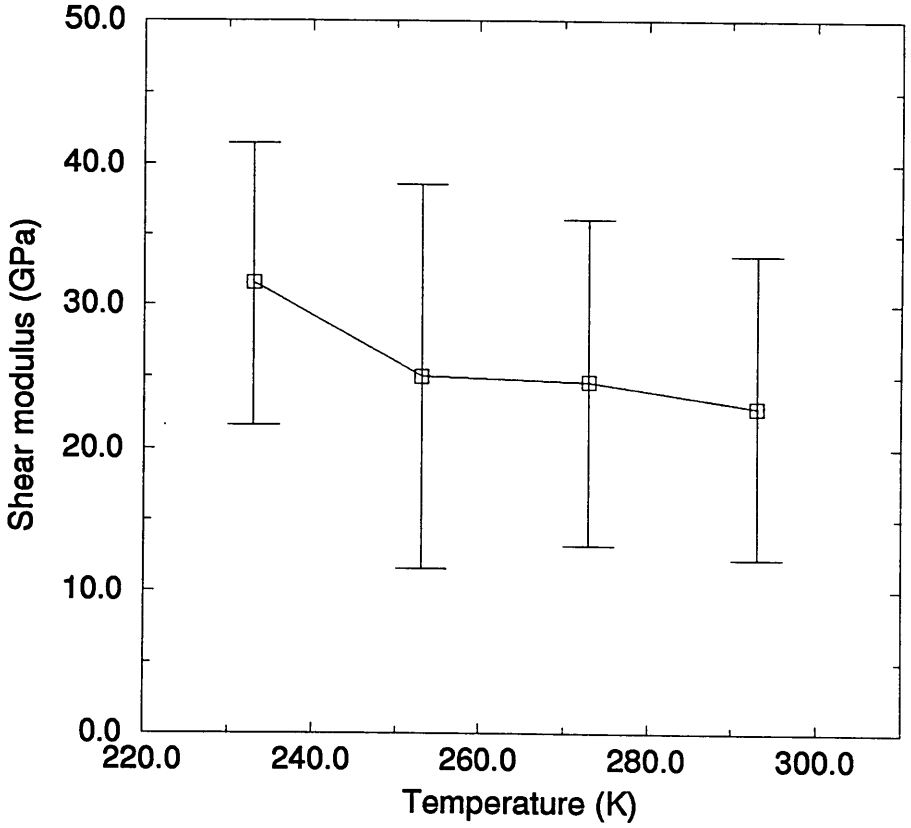

Figure 4-3: Temperature dependence of shear modulus

Table 4.1: Literature values for the shear modulus of polyethylene (GPa)

C_{55}	Temperature (^oC)	Reference	Method
0.98	75	[48]	Exp.
1.60	0	[49]	Exp.
1.80	-60	[50]	Exp.
0.88		[51]	Theo.
1.98		[52]	Theo.
1.62		[53]	Theo.

modulus from the infinite chain model, but still well above the experimental values. However the bilayer chain model exhibited a totally different deformation behavior (see Section 4.2) making it difficult to conclude that the infinite length of the chain is alone the reason for the very high modulus observed. Other possible explanations are that the simulation cell size is still too small or that significant time dependent viscoelastic phenomena are not captured by these short time simulations.

The apparent yield stresses were calculated at 233^oK, 273^oK and 293^oK. Because of the use of the finite stress increments, it's hard to say the exact stress at which the slip begins. But a lower limit for the stress at which yield is observed was obtained. It was found to be $1.5GPa$ at 233^oK, $1.375GPa$ at 273^oK and $1.24GPa$ at 293^oK. The elastic strain was found up to $6 \sim 7\%$ in these simulations. The system could remain at the so-called "yield stress" for as long as 30 ps without showing any sign of slip. However the system could yield at a lower stress at longer times because plastic deformation is a time consuming process. The rate at which slip occurs, i.e. dislocations or other defects are generated, depends on the stress. Since the time studied is very short, high stress is needed to make slip process occur in that time span. These yield stresses are very high even for metals, but are not unreasonable considering the small simulation cell size, the perfectness of the chain model and the short time simulated. Indeed, the calculated yield stresses from the perfect infinite chain model are the ideal mechanical thresholds for plastic deformation, which is very high for covalent materials. As for the defected model (see Section 4.6), the calculated yield stresses are only one stress increment unit ($27.5MPa$) lower than the results from perfect model. This is because those chain rotational defects are relatively local

defects compared to the usual sources of dislocations, such as crystal boundaries, Frank-Read sources, etc. which are the main reason for materials having a much lower yield stress than the ideal mechanical threshold. For the bilayer chain model, a totally different deformation process was found (see Section 4-2), accordingly there was a different yield stress ($825.16MPa$).

4.6 Chain Slip and Generation of Screw Dislocations

In this section, results obtained under the same applied stress and the same temperature (273^oK) but with different models will be presented. One model is a perfect crystallographic structure and the other contains defects of the type described in Chapter 3. For convenience, the perfect model is called "Model I" and the defected model "Model II". Both are infinite chain models. Figure 4-4 shows a view of "Model II" along the chain axis. In this model, 5 of the 24 chains are rotated about their axis approximately -90^o from their lowest energy positions as one can estimate from the picture. It was believed that these rotated chains are in the next lowest minimum position described in Chapter 3. However the defects in the MD simulation always occurred in at least pairs. It appears that this changes the position of the minimum from the -70^o observed for an isolated defect.

Two "movies", with one from "Model I" and the other from "Model II", showing how the system changed from nonslipped states to slipped states are given in Figure 4-5. In order to see each chain clearly, the unit cell is rotated about the z-axis $1 \sim 2^o$. From the movies one can clearly see that these two models have totally different behaviors under the same applied stress. Slip in "Model I" was a perfect inter-planar slip between different atomic planes, whereas in "Model II", a number of screw dislocations were generated in the slip process. Looking at "Model II" in Figure 4-5c, one can find in the left column of four chains that two of them are moving upward and two of them downward indicating two dislocation cores exist in this column of chains. Comparing the structure to the dislocation model in PE proposed by Predecki

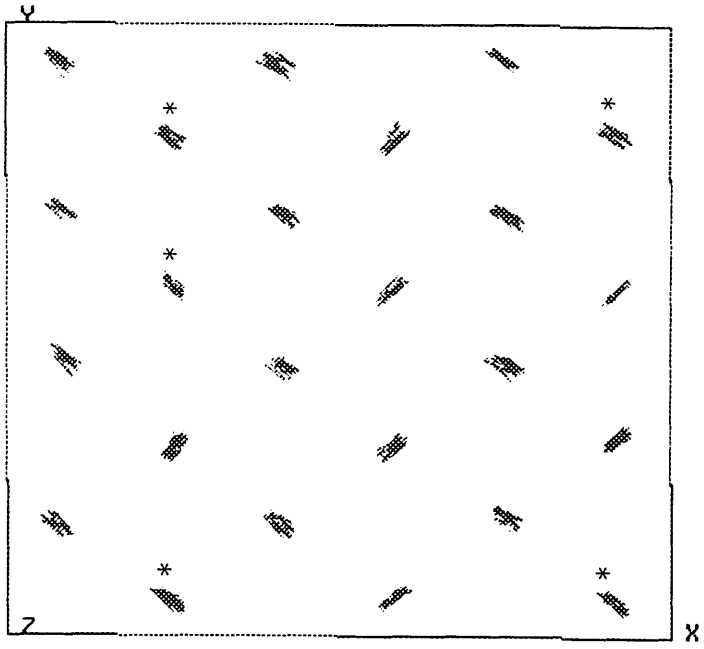

Figure 4-4: A picture of defected infinite chain model: Only C-C bond backbones are shown here. The chains with a star are those away from their lowest energy position.

and Statton (see Figure 1-1c), one can see a clear similarity. Also in the right column of the four chains, one can find another two similar dislocation cores.

For clarity, two different moments of the movie of "Model II" viewed along the z-direction are shown in Figure 4-6. From Figure 4-6 one can see the dislocations were moving. Comparing Figure 4-6 to Figure 4-4, one can find that the dislocations generated in the defected model were located either at the chains with rotational defects or next to them. In addition, the defected model showed a lower yield stress (about one stress increment unit of $27.5MPa$) compared to the perfect model. These results clearly indicate the importance of the rotational defected chains in the generation of screw dislocations.

The dislocations observed in the simulations have very small cores. This is most likely due to the small simulation cell used. With PBC every dislocation core has to be repeated for every cell. Thus a small simulation cell results in a very high density of dislocations with a very high repulsive interaction energy and therefore the cores are restricted in size. If the simulation cell size were increased, one would expect the cores to be more extended.

The simulations at other temperatures (233^oK, 293^oK) gave similar results suggesting the results shown in this section are not just an accident and those rotational defects are playing a key role in the process of generation of screw dislocations.

4.7 Potential Energy Changes and Chain Direction Displacements

The calculated potential energy for the system containing defects in the process of slip is shown in Figure 4-7. One can see clearly from the curve that right after the slip happened the system potential energy decreased dramatically, which means that some of the energies were released in the process. Detailed energy analysis showed that the lost energy became the work done on the wall of the system. The curves show exactly the onset time of the plastic process pictured in Figure 4-6.

The chain direction (along z-axis) displacements were calculated by subtracting

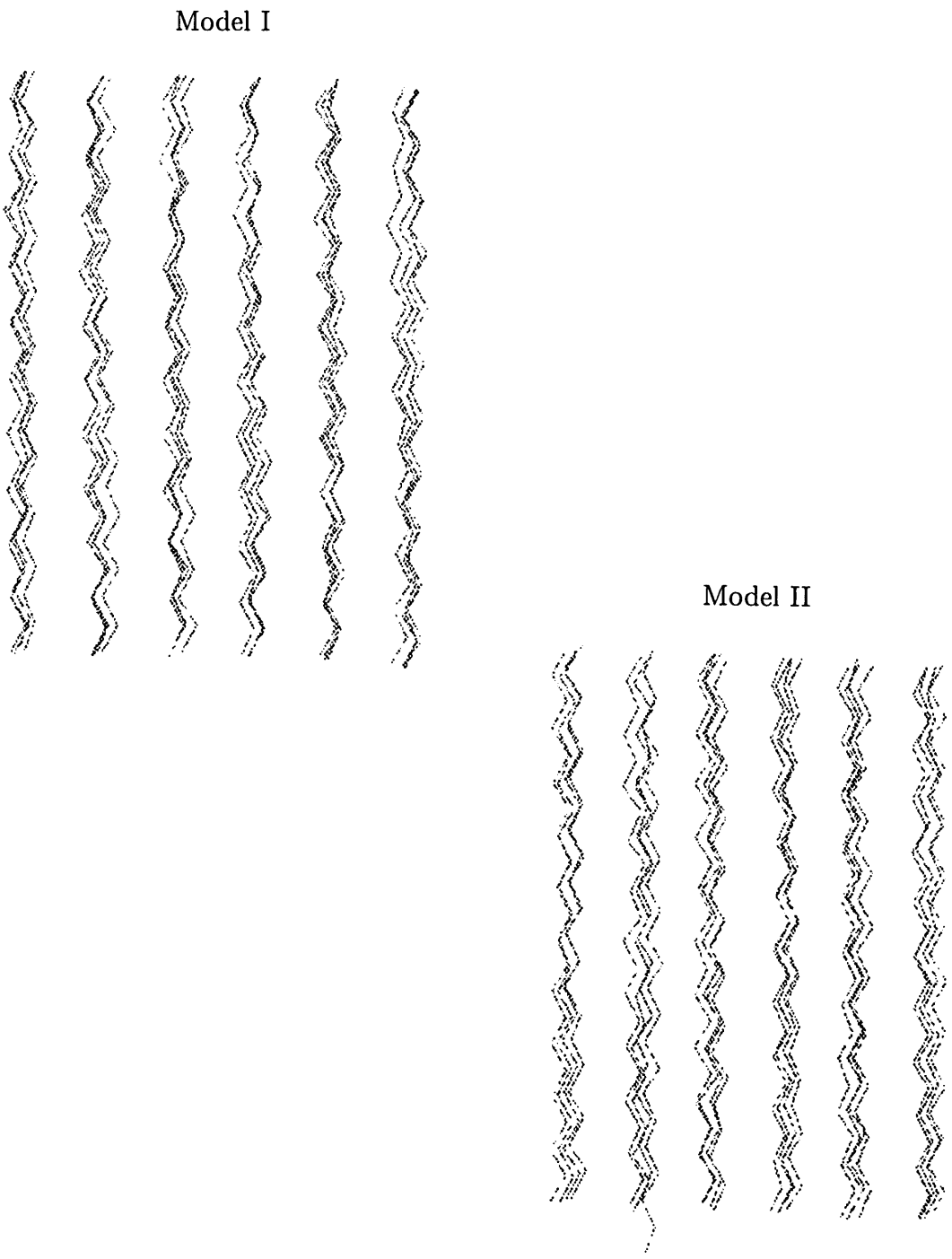

Figure 4-5: Deformation process (movies): (a) The moment right before the slip starts.

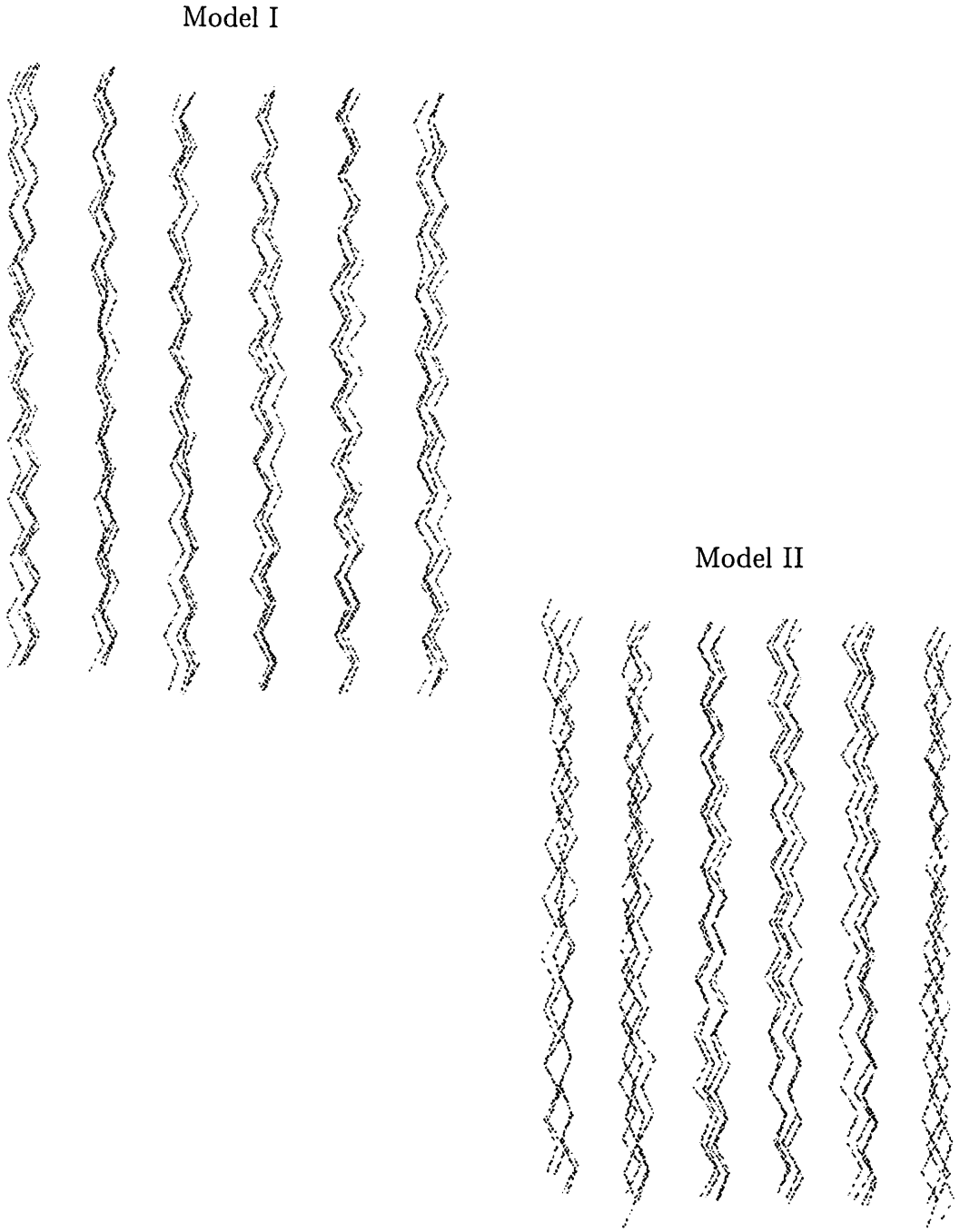

Figure 4-5: Deformation process (movies): (b) Intermediate stage of the slip.

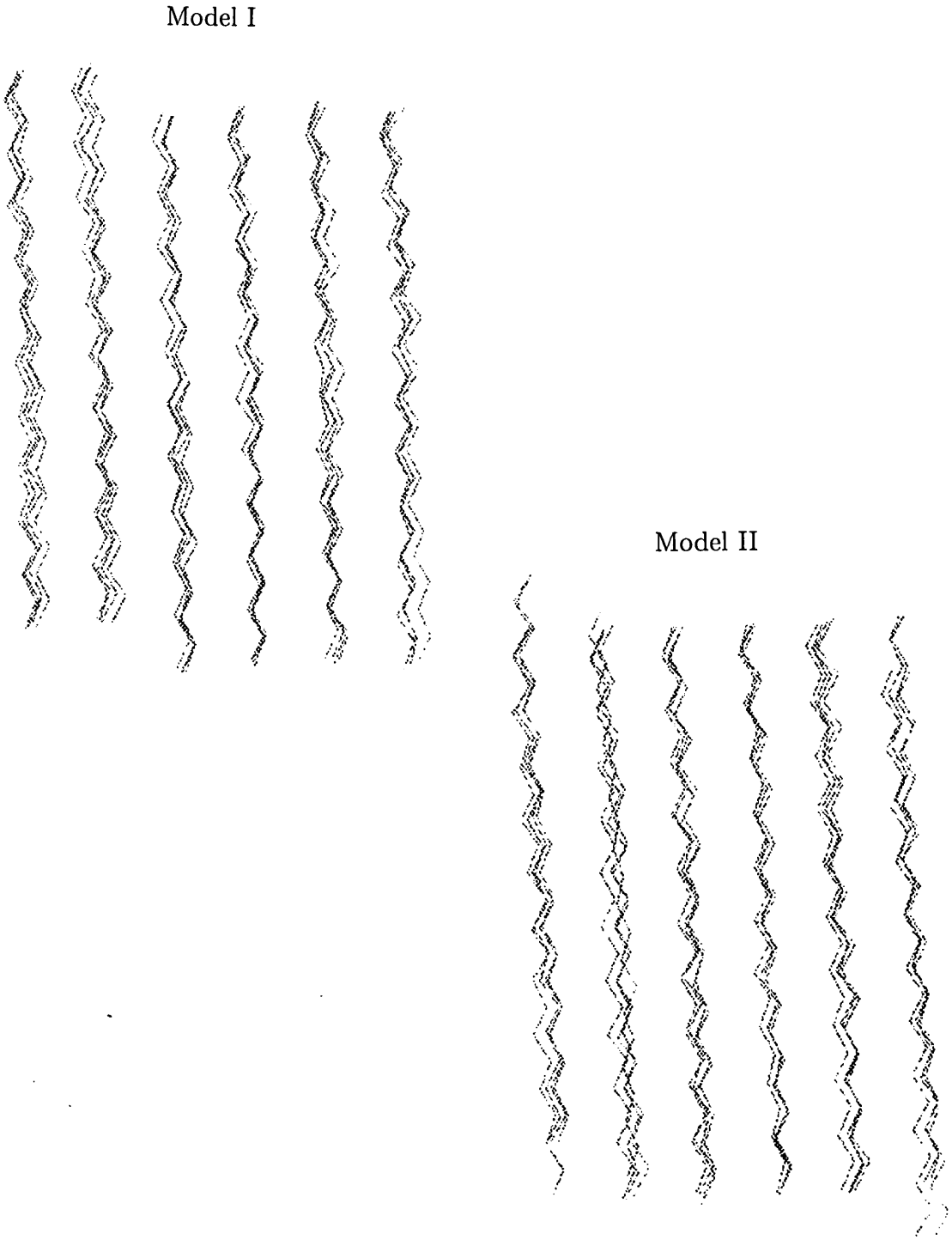

Figure 4-5: Deformation process (movies): (c) Later stage of the process.

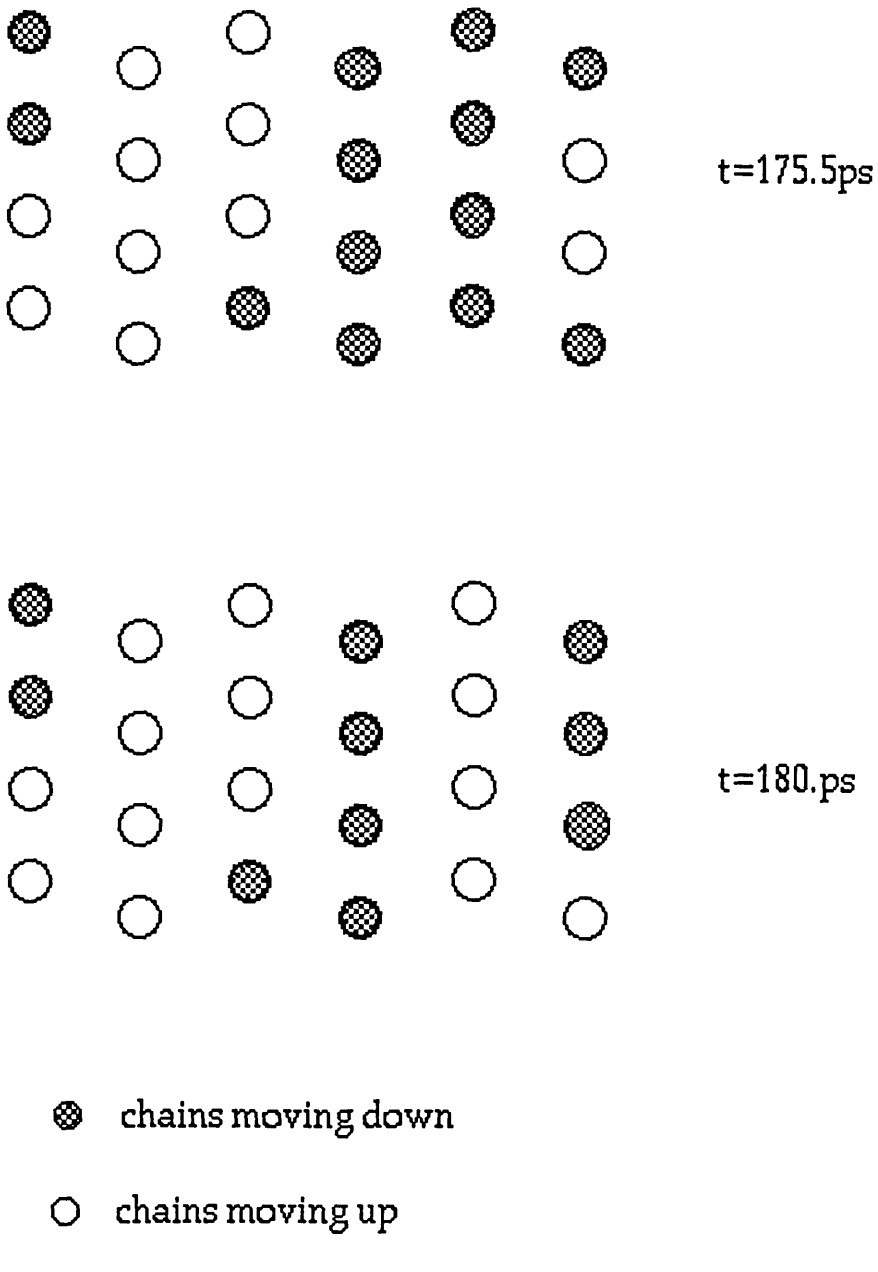

Figure 4-6: Plane picture of the slipped structure

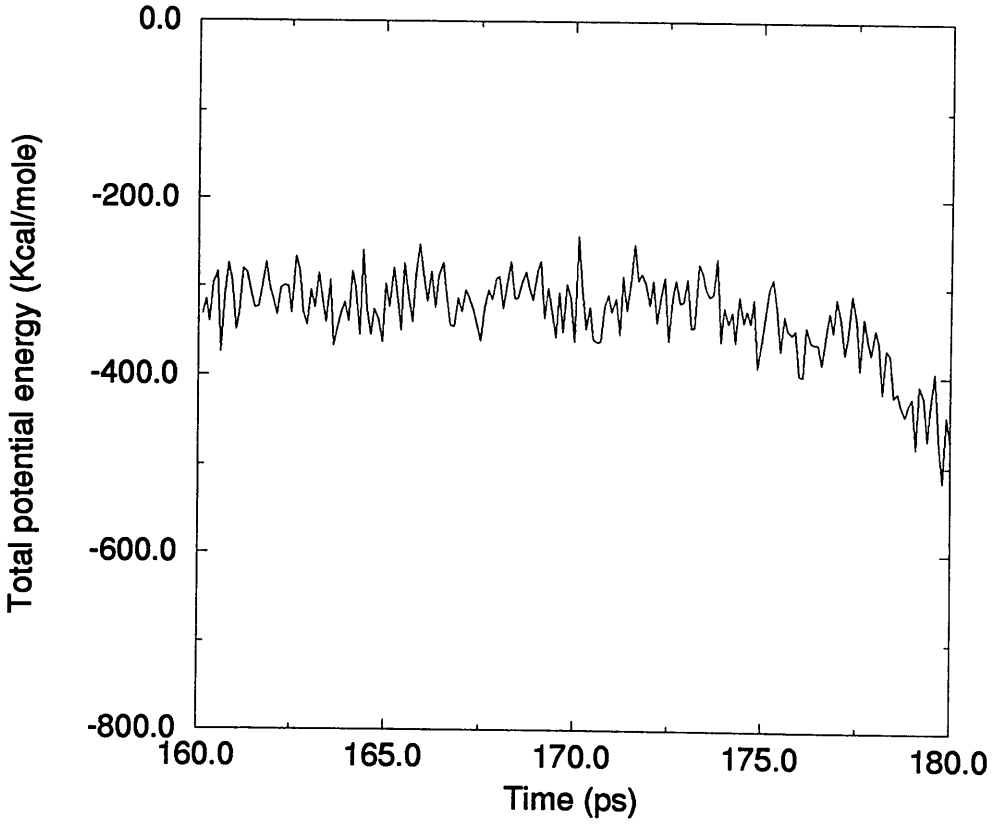

Figure 4-7: Potential energy as a function of time

out the elastic accommodation of the chains to the change of the simulation cell from the total displacement of the chains. Different atoms in the same chains were monitored and the results were found to be similar to each other for the atoms in the same chain. Four atoms in the middle of four different chains (in the same column, see Figure 4-6, these chains are #21, #22, #23 and #24) with typical chain direction displacements are plotted as in Figure 4-8. All calculations were done in the unitless internal coordinates of the cell, therefore the chain direction displacements in Figure 4-8 are also unitless. The real displacements are the value in Figure 4-8 multiplied by the chain length of 22.434 $\AA$. As one can see from Figure 4-8a and b, starting at 173 ps or so, chain #21 and chain #22 begin to climb up and at the same time as in Figure 4-8c and d, chain #23 and chain #24 begin chain #24 begin to slip down relative to the position they were at the beginning of the simulation. This is a clear statement that the plastic deformation process happened.

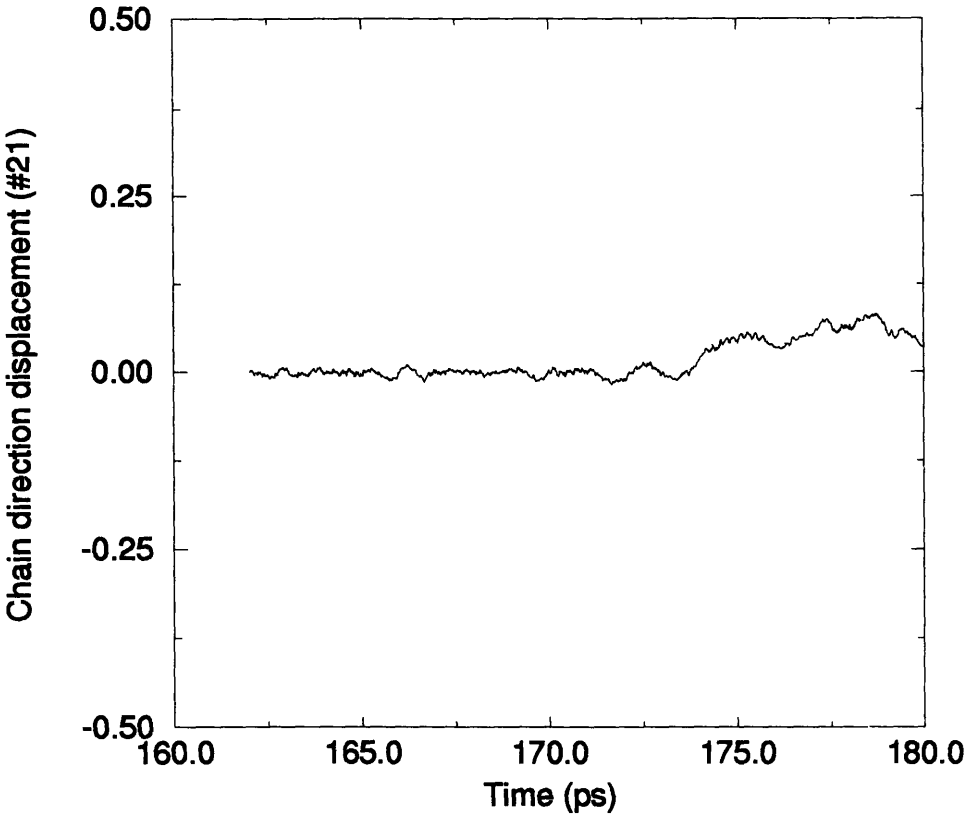

Figure 4-8: Chain direction displacements: (a) chain #21

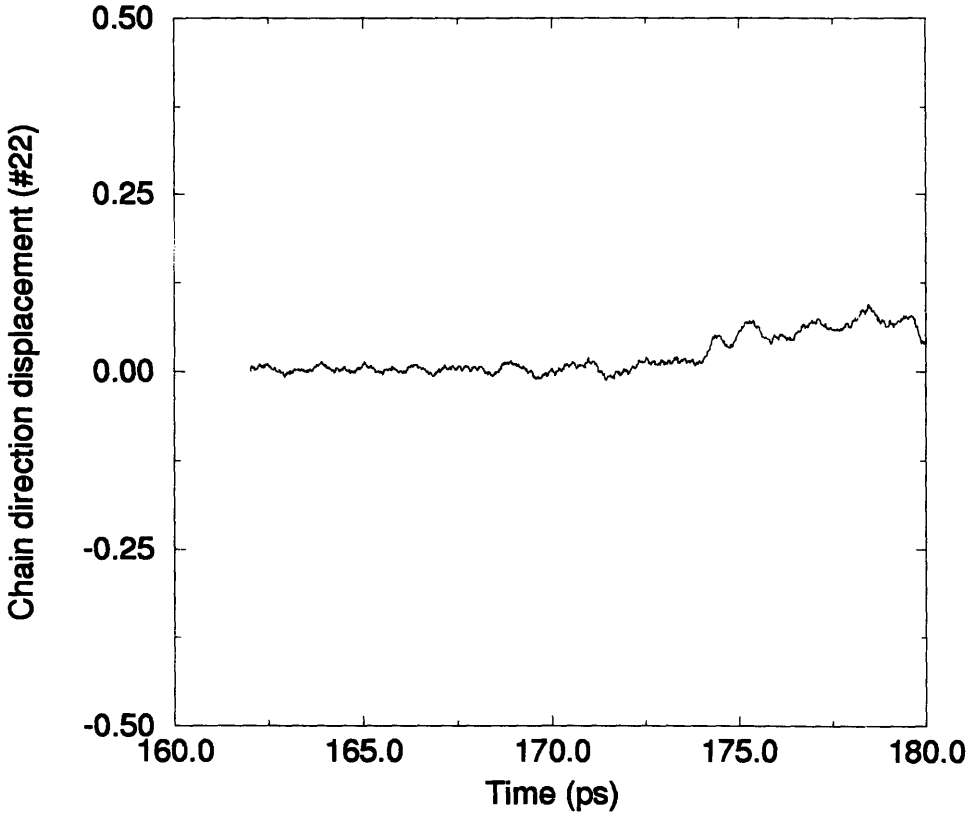

Figure 4-8: Chain direction displacements: (b) chain #22

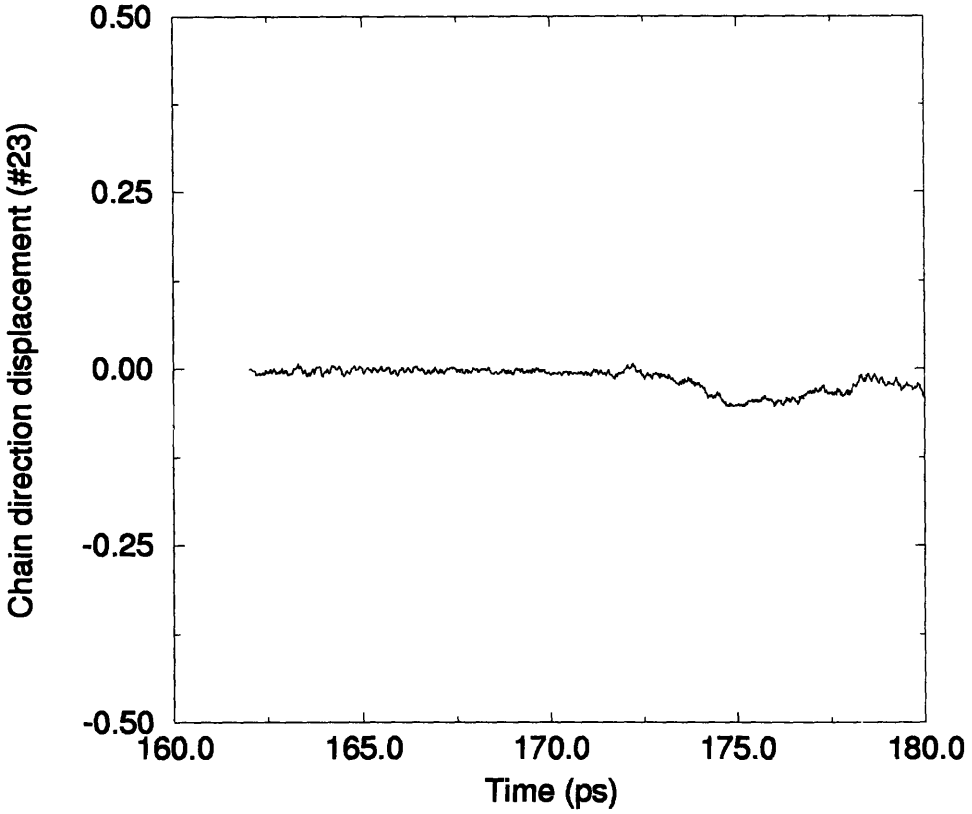

Figure 4-8: Chain direction displacements: (c) chain #23

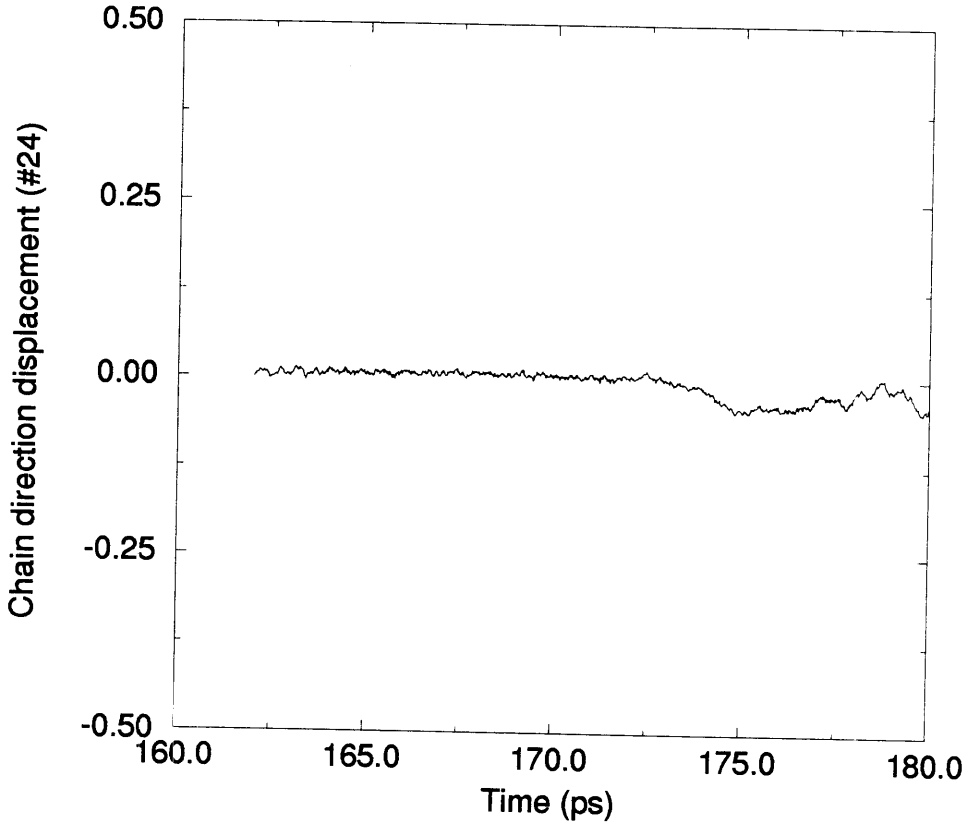

Figure 4-8: Chain direction displacements: (d) chain #24

Chapter 5

Conclusions

5.1 Conclusions

Isothermal-isostress MD calculations have been carried out for an infinite chain model and a bilayer chain model to simulate the plastic deformation process in crystalline PE. Results for the equilibrium properties of crystalline PE showed the model reproduced the behavior of the real material reasonably well.

A room temperature chain rotational defected state was proposed from energy minimization calculations. The population of the defects was calculated and in later MD simulation, it was apparent that this kind of defects can play a key role in the process of plastic deformation in crystalline PE, i.e. the plastic deformation involving chain slip can only be obtained from defected states rather than perfect states.

The plots of potential energy and chain directional displacements showed clearly the onset of plastic deformation. A disappointing result was the failure to observe the formation of chain defects such as "kinks" and "jogs" in the simulation at realistic temperatures even with very high stresses because of the infinite chain model used in this work.

5.2 Future Work

Plastic deformation process in crystalline polymer is a big topic where there are still problems to be solved. The following future work is proposed:

- Analyze atomic stress and strain to obtain local driving forces for the plastic strain producing events and connect the observed atomic motion to macroscopic continuum.
- Map out the potential energy surface to get activation barrier for plastic deformation.
- Separate the atomic motion directly involved in the plastic events from motions which merely represent the elastic accommodation of the other atoms in the system.
- Investigate the formation and movement of various crystal defects and introduce these defects into simulation model to see how they affect the plastic deformation process.
- Investigate the energetics of multiple chain rotational defects.

Bibliography

[1] Bowden, P. B. and Young, R. J., 1974, *J. Mat. Sci.*, vol. 9, pp. 2034.

[2] Roe, R. J., ed. 1991, *Computer Simulation of Polymers*, Prentice Hall, Englewood Cliffs.

[3] Lin, L. and Argon, A. S., 1994, *J. Mat. Sci.*, vol. 29, pp. 294.

[4] Frank, F. C., Keller, A. and O'Connor, A., 1958, *Phil. Mag.*, vol. 3, pp. 64.

[5] Keith, H. D. and Passaglia, E., 1964, *J. Res. Nat. Bur. Stds*, vol. 68(A), pp. 513.

[6] Predecki, P. and Statton, W. O., 1967, *Appl. Polym. Symp.*, vol. 6, pp. 165.

[7] Kiho, H., Peterlin, A. and Geil, P. H., 1965, *J. Polym. Sci.*, vol. B3, pp. 257.

[8] Hay, I. L. and Keller, A., 1965, *Kolloid-Z. Z. Polym.*, ed. 13, pp. 533.

[9] Gleiter, H. and Argon, A. S., 1971, *ibid.*, vol. 24, pp. 71.

[10] Galeski, A., Bartczak, Z., Argon, A. S. and Cohen, R. E., 1992, *Macromolecules*, vol. 25, pp. 5705.

[11] Cowking, A. and Rider, J. G., 1969, *J. Mater. Sci.*, vol. 4, pp. 1051.

[12] Young, R. J., Bowden, P. B., Ritchie, J. M. and Rider, J. G., 1973, *ibid.*, vol. 8, pp. 23.

[13] Allan, P. and Bevis, M., 1980, *Phil. Mag.*, vol. 41, pp. 555.

[14] Oda, T., Nomura, W. O. and Kawai, H., 1965, *J. Polym. Sci.*, vol. A3, pp. 1993.

[15] Shadrake, L. G. and Guiu, F., 1979, Phil. Mag., vol. 39, pp. 785.

[16] Crist, B., 1989, *Polymer Commu.*, vol. 30, pp. 69.

[17] Peterson, J. M., 1968, *J. Appl. Phys.*, vol. 39, pp. 4920.

[18] McCullough, R. L. and Peterson, J. M., 1973, *ibid.*, vol. 44, pp. 1224.

[19] Reneker. D. H. and Mazur, J., 1988, *Polymer*, vol. 29, pp. 3.

[20] Bacon, D. J. and Geary, N. A., 1983, *J. Mat. Sci.*, vol. 18, pp. 853.

[21] Bleha, T., Gajdos, J. and Karasz, F. E., 1990, *Macromolecules*, vol. 23, pp. 4076.

[22] van der Werff, H., van Duynen, P. T. and Pennings, A. J., 1990, *Macromolecules*, vol. 23, pp. 2935.

[23] Argon, A. S., Mott, P. H. and Suter, U. W., 1992, *Phys. Stat. Sol. (b)*, vol. 172, pp. 193.

[24] Hutnik, M. and Argon, A. S., 1993, *Macromolecules*, vol. 26, pp. 1097.

[25] Brown, D. and Clarke, J. H. R., 1986, *J. Chem. Phys.*, vol. 85(5), pp. 2858.

[26] Brown, D. and Clarke, J. H. R., 1991, *Macromolecules*, vol 24, pp. 2075.

[27] Ryckaert, J. and Klein, M. L., 1986, *J. Chem. Phys.*, vol. 85, pp. 1613.

[28] Ryckaert, J., Klein, M. L. and McDonald, I. R., 1987, *Physical Review Letters*, vol. 58, pp. 698.

[29] Sumpter, B. G., Noid, D. W. and Wunderlich, B., 1990, *J. Chem. Phys.*, vol. 93(9), pp. 6875.

[30] Noid, D. W., Sumpter, B. G. and Wunderlich, B., 1990, *Macromolecules*, vol. 23, pp. 664.

[31] Xenopoulos, A., Noid, D. W., Sumpter, B. G. and Wunderlich, B., 1990, *Makromol. Chem.*, vol. 191, pp. 2261.

[32] Noid, D. W., Sumpter, B. G. and Wunderlich, B., 1991, *Macromolecules*, vol. 24, pp. 4148.

[33] Pfeffer, G. A., Sumpter, B. G. and Noid, D. W., 1991, *Polymer Eng. and Sci.*, vol. 32, pp. 1278.

[34] Sumpter, B. G., Noid, D. W. and Wunderlich, B., 1992, *Macromolecules*, vol. 25, pp. 7247.

[35] Mansfield, M. and Boyd, R. H., 1978, *J. Polym. Sci. (Phys.)*, vol. 16, pp. 1227.

[36] Krishna Pant, P. V., Han, J., Smith, G. D. and Boyd, R. H., 1993, *J. Chem. Phys.*, vol. 99(1), pp. 597.

[37] Allen, M. P. and Tildesley, D. J., 1987, *Computer Simulation of Liquids*, Clarendon, Oxford.

[38] Sylvester, M. F., 1992, *Molecular Dynamics Studies of the Liquid-Glass Transition in Atactic Polypropylene*, Ph.D. Thesis, Dept. of Mech. Eng., M.I.T.

[39] Ullo, J. J. and Yip, S., 1986, *J. Chem. Phys.*, vol. 85(7), pp. 4056.

[40] Press, W. H., Flannery, B. P., Teukolsky, S. A. and Vetterling, W. T., 1986, *Numerical Recipes: The Art of Scientific Computing*, Cambridge Univ. Press: Cambridge, United Kingdom.

[41] McCrum, N. C., Buckley, C. P. and Bucknall, C. B., 1988, *Principles of Polymer Engineering*, Oxford Science Publications.

[42] Young, R. J. and Lovell, P. A., 1991, *Introduction to Polymers*, Chapman & Hall.

[43] Boistelle, R., 1980, Current Topics in Materials Science, vol. 4, pp. 413.

[44] McCullough, R. L., 1974, *J. Macromol. Sci. Phys.*, vol. 94, pp. 8426.

[45] Lacks, D. J. and Rutledge, G. C., 1993, *J. Phys. Chem.*, vol. 98, pp. 1222.

[46] Davis, G. T., Eby, R. K. and Colson, J. P., 1970, J. Appl. Phys., vol. 41, pp. 4316.

[47] Maloney, D. P. and Praunitz, J. M., 1974, *J. Appl. Polym. Sci.*, vol. 18, pp. 2703.

[48] Rider, J. G. and Watkinson, K. M., 1978, *Polymer*, vol. 19, pp. 645.

[49] Leung, W. P., Chen, F. F., Choy, C. L., Richardson, A. and Ward, I. M., 1984, *Polymer*, vol. 25, pp. 447.

[50] Choy, C. L. and Leung, W. P., 1985, *J. Polymer Sci., Polymer Phys. Ed.*, vol. 23, pp. 1759.

[51] Odajima, A. and Maeda, T., 1966, *J. Polymer Sci., C*, vol. 15, pp. 55.

[52] Wobser, G. and Blasenbrey, S., 1970, *Kolloid-Z.Z. Polymere*, vol. 241, pp. 985.

[53] Tashiro, K., Kobayashi, M. and Tadokoro, H., 1978, *Macromolecules*, vol. 11, pp. 914.